applied sciences

MDPI

Article

A New Quantitative Evaluation Index System for Disaster-Causing Factors of Mud Inrush Disasters in Water-Rich Fault Fracture Zone

Jianguo Liu [1], Xiao Zhang [1,*], Xianghui Li [2], Zihan Li [1] and Chuanyu Sun [1]

[1] Geotechnical and Structural Engineering Research Center, Shandong University, Jinan 250061, China
[2] School of Civil Engineering, Shandong University, Jinan 250061, China
* Correspondence: sduzhangxiao@sdu.edu.cn

Abstract: The Yonglian tunnel in China has experienced 15 instances of severe water and mud inrush disasters, resulting in a total volume of 53,000 m^3 of gushing water and mud. These disasters have caused irreversible environmental damage, including hilltop collapse and soil erosion. To achieve early warning and early management of such disasters, the paper introduced the Fuzzy Comprehensive Evaluation Method into the Analytic Hierarchy Process to establish a new quantitative evaluation index system for the causal factors. As the evaluation method involves expert participation in scoring, it inherently presents certain subjective elements. To further substantiate the validity of our approach, we conducted a series of model tests. Then, the accuracy of the quantitative evaluation indexes was verified through these model tests, indicating that the quantitative evaluation system has important guiding significance for safe tunnel construction, allowing for early warning and management of potential disasters.

Keywords: mud inrush; analytic hierarchy process; water-rich fault fracture tunnel; model test; disaster-causing factors

Citation: Liu, J.; Zhang, X.; Li, X.; Li, Z.; Sun, C. A New Quantitative Evaluation Index System for Disaster-Causing Factors of Mud Inrush Disasters in Water-Rich Fault Fracture Zone. *Appl. Sci.* **2023**, *13*, 6199. https://doi.org/10.3390/app13106199

Academic Editor: Giuseppe Lacidogna

Received: 11 April 2023
Revised: 15 May 2023
Accepted: 17 May 2023
Published: 18 May 2023

1. Introduction

With the rapid implementation of China's "Belt and Road" strategy, the construction of mountain tunnels has become widespread across the country. However, these tunnels often face the formidable challenge of water and mud inrush disasters, which are exacerbated by the complex geological conditions, including fault fractures and karst areas. The mud outburst process involves a sudden and substantial influx of mud into the tunnel, resulting in significant economic losses and casualties [1–3]. Furthermore, the aftermath of these disasters can lead to irreversible impacts, including soil erosion and mountain collapses, which adversely affect the surrounding environment [4,5]. Incomplete statistics reveal that water and mud inrush disasters account for approximately 45% of geological disasters during tunnel construction in China [6]. These mud inrush disasters pose significant obstacles to the safe and expeditious completion of tunnel construction.

In the field of engineering, risk assessment methods can effectively provide early warning of engineering disasters, reduce the occurrence of disasters, and ensure the safety of property and life. Therefore, risk assessment methods have been widely researched and applied. Ali et al. investigated, quantitatively, the risk of rainfall-induced landslides by assessing the consequence of each failure [7], Orejuela et al. evaluated the susceptibility to landslides through Fuzzy Logic in the Macas-Riobamba road [8], and Kazakis et al. introduces a multi-criteria index to assess flood hazard areas in a regional scale [9]. Different disaster-causing factors have been proposed [10,11], and various risk prediction methods have been suggested [12,13] with the aim of reducing the possibility of water and mud inrush in karst areas.

Various model testing systems have been developed in the field of tunnel stability. For instance, Gregor et al. developed a small-scale tunnel model in a geotechnical centrifuge to investigate the collapse at the tunnel face under different overburden pressures [14]. Soranzo et al. conducted a study on the face stability of shallow tunnels in partially saturated soil using centrifuge testing [15]. Many model testing systems for tunnel water inrush disasters have been established, and these systems are now able to accurately simulate the effects of ground stress and water pressure, achieving realistic simulation results. Some model testing systems are also capable of being reused multiple times, and their results have already proven effective in guiding engineering practices [16–18].

However, most of the existing scholarly research on water and mud disasters has primarily focused on karst areas, where water inrush is the predominant type of disaster, and mud inrush is often considered as an accompanying phenomenon. In contrast, in water-rich fault zones, mud inrush disasters tend to dominate. The characteristics of protrusions, factors causing disasters, and disaster processes in these areas differ significantly from those in karst areas. Moreover, the related mechanisms causing such disasters, methods for risk evaluation, and physical model experimental approaches also vary greatly. As a result, research in this particular area is still scarce and inadequate.

Hence, conducting a specialized study on mud inrush disasters in water-rich fault fracture zones is imperative. In this paper, the Yonglian tunnel mud inrush disasters are taken as an example, and the Analytic Hierarchy Process (AHP) methodology is employed to assess the relative importance of various factors contributing to these disasters. Furthermore, a series of model tests are conducted to qualitatively verify the theoretical findings under different conditions. The results of this evaluation system have implications for the prevention and mitigation of mud inrush disasters in water-rich fault fracture zones.

2. Case of Mud Inrush Disaster

2.1. Engineering Situation and Disaster Overview

The Yonglian Tunnel, situated in Jiangxi Province, China (Figure 1), is a split tunnel spanning 2500 m in length. It traverses a mountainous and hilly region characterized by rolling topography. The tunnel area is known for its subtropical monsoon climate, resulting in groundwater with an average depth of approximately 50 m. Notably, the tunnel intersects a significant fault known as the F2 fault, which spans 520 m with an inclination of 84 degrees, from K91 + 350 to K91 + 368.

Figure 1. Location of the tunnel.

The F2 fault, however, has been significantly impacted by long-term weathering and tectonic activity, resulting in extensive fragmentation and weathering. It contains a substantial amount of mylonite, breccia, and fault mud, with a rock quality designation (RQD) of less than 5%. These geological characteristics indicate the poor quality of the rock mass in the F2 fault zone, posing formidable challenges for tunnel construction in this area.

During the preliminary geological investigation, there was a severe lack of accurate information regarding the F2 fault, and the geological report indicated that the intersection length between the F2 fault and the tunnel was only 5 m, far less than the actual length of 18 m. Additionally, the strength of the surrounding rock did not match the actual excavation conditions. As a result, more cautious excavation and support methods were not adopted during construction, nor were more precise disaster control methods employed.

When the tunnel excavation neared the F2 fault using a three-step excavation method, a large number of geological hazards occurred, resulting in the suspension of tunnel construction for a period of 2 years and causing substantial economic losses. Initially, there were four small-scale collapses that occurred intermittently, resulting in deformations of the surrounding rock and cracks in the lining. In response, treatment measures such as pipe roof grouting and small pipe grouting were implemented to mitigate the gushing water and reinforce the broken surrounding rocks. Subsequently, tunnel construction resumed.

However, just seven days later, the first mud inrush disaster occurred suddenly, with substantial amounts of mud–water mixtures inundating the tunnel. Although construction workers had detected significant deformation of the tunnel surrounding rocks in advance and identified the risk of instability, the mud inrush disaster occurred too violently and quickly for them to take measures to prevent it. This was followed by a total of 15 enormous mud inrush disasters that occurred successively within a span of four months (as shown in Table 1). It was estimated that approximately 53,000 m^3 of mud–water mixture gushed into the tunnel in total, resulting in nearly 30 m of the constructed tunnel being inundated. These disasters triggered a series of engineering accidents, including equipment damages, large-scale collapses, and construction interruptions [19].

Table 1. Large-scale mud inrush disasters.

Order	Date	Mixture Volume/m^3	Order	Date	Mixture Volume/m^3
1	2 July 2012	1000	9	9 August	300
2	3 July	4000	10	19 September	3000
3	5 July	20,000	11	23 September	2900
4	15 July	1100	12	1 October	1100
5	24 July	4000	13	2 October	900
6	12 August	1000	14	7 October	4000
7	13 August	400	15	25 October 2012	8000
8	15 August	1300			

Furthermore, a collapse pit with an area of about 2000 m^2 emerged at the mountain peak after the continuous disasters (as shown in Figure 2), resulting in severe vegetation destruction and soil erosion. The engineering geological schematic diagram is shown in Figure 3 [3].

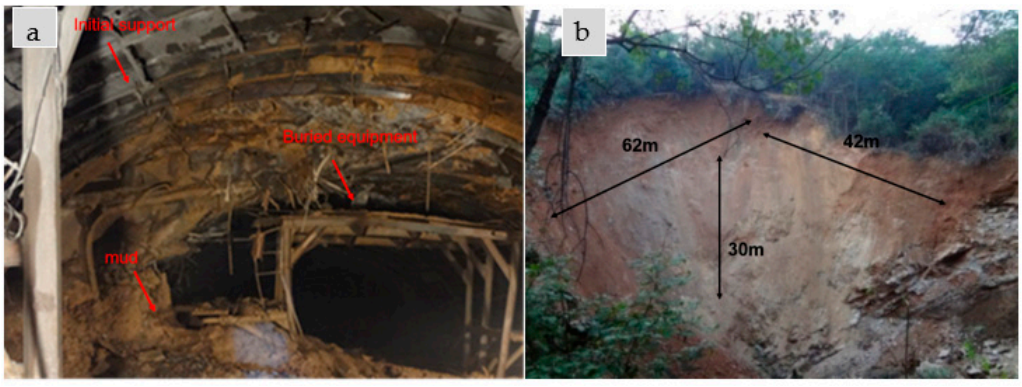

Figure 2. Partial mud inrush disasters and the collapse pit. (**a**). Mud inrush disaster in tunnel. (**b**). Collapse pit at the mountain peak.

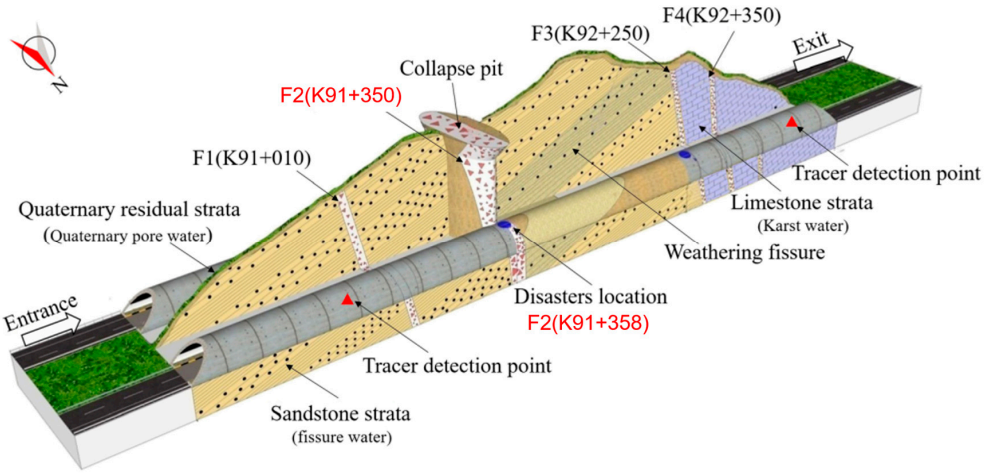

Figure 3. Engineering geological schematic diagram.

2.2. Disaster Causes

The mud inrush disasters were a dynamic destruction hazard caused by excavation disturbances. Based on the results of the engineering geological investigation, the presence of ample groundwater and broken surrounding rocks in the F2 fault created favorable conditions for these disasters.

First and foremost, the characteristics of the F2 fault in the mountain surface were large depressions whose terrain was obviously lower than that of those in other places. Hence, a great deal of rainwater or groundwater would gather in the area. Subsequently, there were a large number of fissures among the loose and broken surrounding rocks in the F2 fault, which provided the groundwater with convenient migration pathways and plentiful storage space. As a consequence, the accumulated water could flow down the migration pathways into the mountain interior easily and was stored in the fissures. It is noteworthy that the stored groundwater would develop into confined water gradually as time went on, and a great deal of potential energy was accumulated in the groundwater and nearby surrounding rocks. Furthermore, when the groundwater began to flow, the weakened and unstable surrounding rocks in the F2 fault were unable to withstand the groundwater erosion, resulting in easy erosion and disintegration. Last but not least, the fault mud typically contained various hydrophilic clay minerals such as montmorillonite and illite, meaning that the surrounding rocks in the F2 fault would be very easy to swell and disintegrate, turning into weakened and deformable rocks with worse physical and mechanical properties under the effects of groundwater.

Although all varieties of natural conditions had been available, mud inrush disasters rarely occurred before excavations, as the majority of groundwater remained stable under the balance of water pressure, rock stress, and tectonic stress. However, during tunnel excavation, the previously stable equilibrium state between water and rock was disrupted. This led to an increasing number of fissures extending towards the tunnel face due to stress distribution, resulting in active and accelerated groundwater seepage. Additionally, the broken surrounding rocks in the F2 fault were continuously flushed by the active groundwater, causing the migration pathways to gradually enlarge.

However, due to inaccurate geological surveys in the early stages, a correct understanding of the danger level of the F2 fault was absent. During the construction phase, conventional three-step excavation methods and simple stability monitoring measures were employed, without using methods such as grouting to reinforce the surrounding rock. Subsequently, the expanded migration pathways led to persistent increases in seepage velocity and pressure, intensifying the loss of surrounding rocks. As the pathway expansions and particle migrations aggravated, the tunnel face eventually connected to groundwater. Unable to resist the energy released by the groundwater and the surrounding

rocks, the frail tunnel face gave way, leading to mud–water mixtures instantly pouring into the tunnel. Furthermore, due to the sustained interrelationship between the seepage field and stress field, the mud–water mixtures continued to flow from the F2 fault without stopping, resulting in repeated mud inrush disasters.

2.3. Disaster-Causing Factors of Mud Inrush Disasters

Taking into account the underlying causes of mud inrush disasters, it can be concluded that groundwater serves as a significant driving force, while the fractured surrounding rocks provide migration pathways for the groundwater. Additionally, the weakened rocks in the fault fracture zone act as material sources for these disasters. Moreover, excavation disturbances are unequivocally identified as direct triggers of such disasters. Therefore, the factors that contribute to the occurrence of mud inrush disasters are closely intertwined with groundwater dynamics, characteristics of the surrounding rocks, and tunnel construction activities. Based on the foregoing analyses, the disaster-causing factors were categorized as follows.

2.3.1. Geological Factors

1. Terrain

The low-lying areas, such as gullies and hollows, provide convenient sites for the aggregation of rainwater, which serves as the primary recharge source for groundwater. As a result, there exists a significant linkage between the terrain characteristics and the occurrence of mud inrush disasters.

2. Physical and mechanical properties of fault-surrounding rocks

The fissures and voids among the fault-surrounding rocks play a crucial role in providing migration pathways and storage space for groundwater, and their characteristics such as porosity, density, and pore structure are closely related to the stability of the fault zone. It can be inferred that fault-surrounding rocks with high porosity and loose structure are conducive to the migration and storage of groundwater, increasing the likelihood of mud inrush disasters. Furthermore, the strength characteristics of fault-surrounding rocks, including compression strength, shear strength, and elastic modulus, are critical in determining their stability under dynamic groundwater conditions. High-strength rocks are less likely to lose stability easily and are more resistant to erosion by flowing groundwater due to their passable strength and stability. These rocks can effectively withstand the potential energy released by groundwater, reducing the risk of mud inrush disasters. In contrast, fault-surrounding rocks with poor strength characteristics are highly prone to causing disasters. Predictably, the occurrence of mud inrush disasters is closely correlated with the strength and stability of fault-surrounding rocks, as well as their porosity and structure.

3. Fault scale

The fault mud, gravel soil, and tiny breccia that originate from the fault zone serve as the main source of the gushing mud during mud inrush disasters. The severity of these disasters is closely related to the scale of the fault. It can be deduced that larger faults would provide more fillers, thus exacerbating the disasters. Furthermore, larger faults are likely to have more migration pathways and storage space, which can further contribute to the occurrence and severity of mud inrush disasters.

2.3.2. Hydrologic Factors

1. Climate

As mentioned previously, the groundwater that drives the mud inrush disasters is primarily supplied by rainfall, which is closely linked to climate conditions. Therefore, the occurrence of these disasters is inherently connected to the climate. For instance, during rainy seasons, continuous heavy rainfall can cause the groundwater level and hydrostatic

pressure to rise continuously. As a result, a significant amount of energy can accumulate in the fault zone, potentially leading to catastrophic disasters. Conversely, if the tunnel construction takes place during dry seasons when evaporation exceeds recharge, there may not be enough groundwater to trigger the disasters.

2. Groundwater pressure

The groundwater pressure, encompassing both hydrostatic pressure and dynamic water pressure, serves as the driving force for mud inrush disasters. The hydrostatic pressure gradually compresses the surrounding rocks, resulting in the accumulation of stress energy over time. Additionally, the fissures and pores within the rocks may expand under the compressive stress, facilitating groundwater seepage.

Moreover, the dynamic water pressure exerts both impact force and drag force on the surrounding rocks. The impact force weakens the strength of the rocks, making them more susceptible to deformation and failure. The drag force, on the other hand, enables the transfer of rock particles along with the flowing groundwater. In essence, the groundwater pressure contributes to the accumulation of energy, expansion of channels, and migration of particles, all of which have a profound effect on the occurrence of mud inrush disasters.

3. Chemical properties of groundwater

The chemical properties of groundwater, including iron exchange, dissolution, hydration, and hydrolysis, can significantly impact the mineral composition of surrounding rocks. Such chemical actions can result in altered mineral compositions, leading to changes in the structure of the rocks, which in turn affect their strength and stability. As a result, there exists a close relationship between the chemical properties of groundwater and the occurrence of mud inrush disasters.

2.3.3. Human Factors

1. Survey and design

Due to limitations in survey technologies or instruments, it is possible that some crucial engineering geological information may not be accurately acquired during the actual engineering process. This can result in potentially unreasonable tunnel designs. In such cases, there is a high likelihood of mud inrush disasters occurring if the tunnel is constructed without proper consideration of the accurate engineering geological information. The lack of detailed geological survey during the early stages was an important factor in the disaster's occurrence.

2. Construction method

During the tunnel construction process, excavation disturbances can cause deformations in the surrounding rocks, leading to potential instability and triggering geological hazards. However, the use of appropriate excavation methods can partially reduce these disturbances, and suitable support methods can resist large deformations, thereby enhancing the stability and bearing capacity of the surrounding rocks. As a result, the probability of disasters can be effectively reduced by adopting proper construction methods that take into consideration the actual geological characteristics.

3. Theoretical Analysis of the Disaster-Causing Factors

Indeed, the mud inrush disaster is influenced by various factors as discussed previously, and the contribution of each factor may vary significantly. It may not be feasible to consider all factors comprehensively in practical engineering, especially in the context of disaster treatment. Therefore, a key task in further research, including the study of catastrophic mechanisms and disaster treatment, is to clarify the relative importance of these factors. Quantitative evaluation and ranking of the disaster-causing factors based on their individual significance can help in achieving this objective. By assigning appropriate weights or scores to each factor, a quantitative assessment can be conducted to determine their relative importance in the occurrence and severity of mud inrush disasters. This can

provide valuable insights for effective disaster prevention, mitigation, and management strategies in tunnel construction and other engineering projects.

Indeed, the analytic hierarchy process (AHP), which uses weighted values as the ratio scale, is a reliable tool for quantitatively prioritizing interdependent factors. It has been widely employed in the field of geological hazards [8,20,21], including mud inrush disasters. Accordingly, we integrated the Fuzzy Comprehensive Evaluation Method into the Analytic Hierarchy Process to establish a quantitative evaluation index system for the causal factors, which allows for a quantitative evaluation and ranking of these factors based on their individual significance.

3.1. Presentation of a Hierarchy Model

According to the information in Section 2.3, the hierarchy model of the disaster-causing factors is illustrated in Figure 4, which consists of the goal A, the first-level evaluation indices A_i and the second-level evaluation indices A_{i-j}.

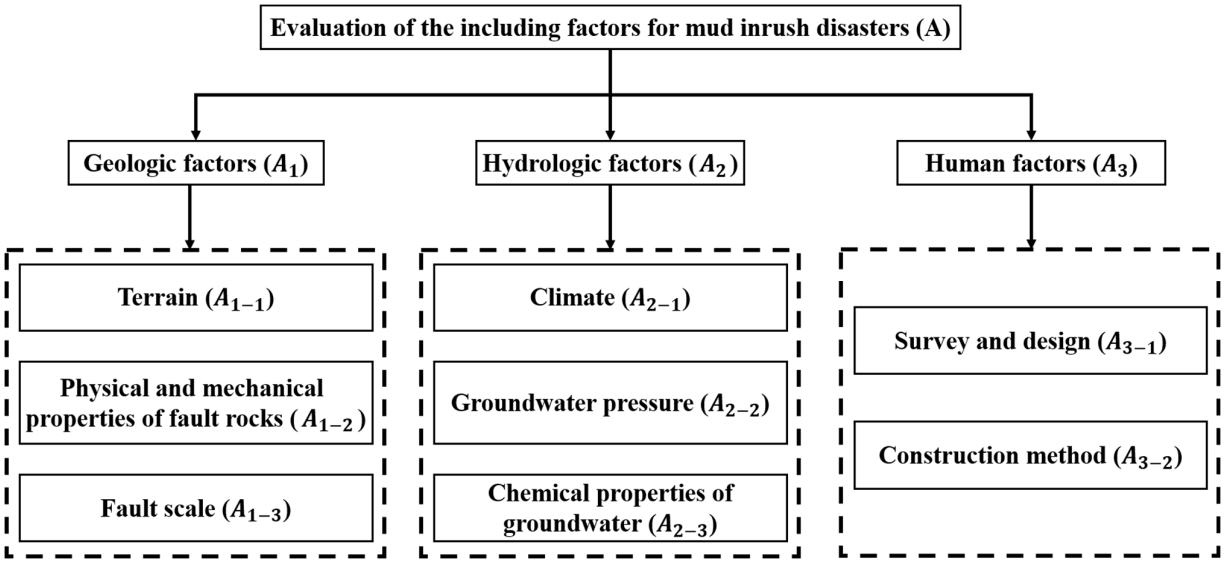

Figure 4. Hierarchy model of disaster-causing factors.

3.2. Determination of Relative Weights

The relative weights, which represent the priorities of the homogeneous indices with respect to the elements at the adjacent upper level, were obtained from the judgment matrices created through pair-wise comparisons.

3.2.1. Judgement Matrix

The indices belonging to the same level and branch in the hierarchical structure were compared as pairs based on their impact on the elements above them. This pair-wise comparison was conducted by a panel of experts using the 1–9 scale thinking method (Table 2). The results of the pair-wise comparisons were collected and used to create the judgment matrices for each level in the hierarchy.

Table 2. The 1–9 scale thinking method for pair-wise comparison.

Value	Explanation
1	Two indices have the same importance
3	One index is moderately important over another index
5	One index is strongly important over another index
7	One index is very strongly important over another index
9	One index is extremely strongly important over another index
2, 4, 6, 8	Intermediate values of two adjacent judgements

3.2.2. Calculation of Weights at Each Level

The relative weights of indices at each level could be denoted by the eigenvectors which are calculated from the judgment matrices using the summation method as described below.

(1) Every judgement matrix a creates a corresponding normalized matrix $\overline{w}$ whose elements are calculated using Equation (1),

$$\overline{w_{ij}} = a_{ij} / \sum_{i=1}^{n} a_{ij}, \quad (1)$$

where $\overline{w_{ij}}$ is the element of the normalized matrix $\overline{w}$ and a_{ij} is the element of the corresponding judgement matrix a.

(2) The elements of the weight matrix w are the eigenvectors which are obtained by Equations (2) and (3),

$$w_i = w_i' / \sum_{i=1}^{n} w_i', \quad (2)$$

$$w_i' = \sum_{j=1}^{n} \overline{w_{ij}}, \quad (3)$$

where w_i is the element of the weight matrix w and w_i' is the element of the transitional matrix w' used for eigenvector calculation.

(3) After obtaining the eigenvectors, it is important to test the consistency of the judgement matrices by calculating the consistency ratio (CR). A CR value of less than 0.1 indicates that the subjective judgments from the experts during the pair-wise comparisons are logical and trustworthy. In such cases, the obtained eigenvectors can be used to denote the relative weights for ranking. However, if the CR value is greater than 0.1, it indicates an inconsistency in the judgments, and the experts should revisit the pair-wise comparisons and make necessary adjustments until the results meet the consistency criterion. The CR is computed as follows:

$$CR = \frac{CI}{RI}, \quad (4)$$

$$CI = (\lambda_{\max} - n)/(n-1), \quad (5)$$

$$\lambda_{\max} = \frac{1}{n} \sum_{i=1}^{n} \frac{(aw)_i}{w_i} \quad (6)$$

where CI is the consistency index, RI is the random consistency index which can be determined according to Table 3, $\lambda_{\max}$ is the maximum eigenvalue and n is the order number of judgement matrix.

Table 3. The value of random consistency index RI.

Order	1	2	3	4	5	6	7	8	9
RI	0.00	0.00	0.58	0.90	1.12	1.24	1.32	1.41	1.45

Finally, the judgment matrices and the relative weights for each index are obtained, as presented in Tables 4–7.

Table 4. Judgement matrix and relative weights of index A_i.

	A_1	A_2	A_3	**Relative Weights**
A_1	1	1	5	0.4545
A_2	1	1	5	0.4545
A_3	1/5	1/5	1	0.0910
$\lambda_{\max}$ = 2.992, n = 3, CI = 0.0000, RI = 0.58, CR = 0.0000 < 0.1				

Table 5. Judgement matrix and relative weights of index $A_{1\text{-}j}$.

	$A_{1\text{-}1}$	$A_{1\text{-}2}$	$A_{1\text{-}3}$	Relative Weights
$A_{1\text{-}1}$	1	1/4	1/3	0.1226
$A_{1\text{-}2}$	4	1	2	0.5572
$A_{1\text{-}3}$	3	1/2	1	0.3202
$\lambda_{max} = 3.0183$, $n = 3$, $CI = 0.0092$, $RI = 0.58$, $CR = 0.0158 < 0.1$				

Table 6. Judgement matrix and relative weights of index $A_{2\text{-}j}$.

	$A_{2\text{-}1}$	$A_{2\text{-}2}$	$A_{2\text{-}3}$	Relative Weights
$A_{2\text{-}1}$	1	1/5	1/2	0.1180
$A_{2\text{-}2}$	5	1	4	0.6806
$A_{2\text{-}3}$	2	1/4	1	0.2014
$\lambda_{max} = 3.0247$, $n = 3$, $CI = 0.0123$, $RI = 0.58$, $CR = 0.0213 < 0.1$				

Table 7. Judgement matrix and relative weights of index $A_{3\text{-}j}$.

	$A_{3\text{-}1}$	$A_{3\text{-}2}$	Relative Weights
$A_{3\text{-}1}$	1	3	0.7500
$A_{3\text{-}2}$	1/3	1	0.2500
Second order matrix is always consistent, no need to test its consistency ($RI = 0$)			

3.3. Comprehensive Evaluation

The relative importance of disaster-causing factors to the mud inrush disasters is characterized by comprehensive weights which are calculated by multiplying the relative weight of every second-level index $A_{i\text{-}j}$ with the relative weight of their corresponding first-level index $A_{i.}$ Accordingly, the comprehensive weights are shown in Table 8.

Table 8. Comprehensive weights of disaster-causing factors to mud inrush disaster.

	A_1 (0.4545)	A_2 (0.4545)	A_3 (0.0910)	Comprehensive Weights
$A_{1\text{-}1}$	0.1226	—	—	0.0557
$A_{1\text{-}2}$	0.5572	—	—	0.2533
$A_{1\text{-}3}$	0.3202	—	—	0.1455
$A_{2\text{-}1}$	—	0.1180	—	0.0536
$A_{2\text{-}2}$	—	0.6806	—	0.3093
$A_{2\text{-}3}$	—	0.2014	—	0.0915
$A_{3\text{-}1}$	—	—	0.7500	0.0683
$A_{3\text{-}2}$	—	—	0.2500	0.0228

The results reveal that the weights of the disaster-causing factors decrease in the following order: $A_{2\text{-}2} > A_{1\text{-}2} > A_{1\text{-}3} > A_{2\text{-}3} > A_{3\text{-}1} > A_{1\text{-}1} > A_{2\text{-}1} > A_{3\text{-}2}$. Notably, the weights of the first three factors are significantly higher than those of the others, with a total weight of 0.4545. This indicates that groundwater pressure, physical and mechanical properties of fault surrounding rocks, and fault scale are the major contributing factors to mud inrush disasters. Therefore, these three factors should be assigned higher priority and greater attention in similar circumstances. Inadequate geological surveys and incorrect construction methods are also significant factors that contribute to the occurrence of the disaster. We should also pay enough attention to human factors in these disasters.

4. Model Test

However, the results obtained using the AHP methodology may be subject to criticism due to the subjective nature of pair-wise comparisons which rely on expert judgments and may lack objectivity. To address this potential drawback, a series of model tests were

conducted to qualitatively verify the theoretical results. These model tests simulated mud inrush disasters under different conditions. Considering the test costs and feasibility, only the three major factors were chosen as test objects. The model tests employed orthogonal testing with three factors and three levels, as well as extremum difference analysis, to study the impacts of different factors on the disaster.

4.1. Test Parameters

4.1.1. Engineering Parameters

The section of the tunnel from K91 + 332 to K91 + 392, which includes the F2 fault (K91 + 350~368), was selected for the model tests. The simulated area covered a total length of 60 m, with a tunnel diameter of 9 m and a distance of 27 m between the center of the left tunnel and that of the right tunnel. The average depth of burial for the tunnel was approximately 180 m. The characteristics of the samples were investigated by conducting coring tests using a core drilling rig. Subsequently, the physical and mechanical properties of the core samples were tested in a laboratory. The key physical and mechanical properties of the surrounding rocks are summarized in Table 9.

Table 9. Main physical and mechanical properties of surrounding rocks.

	Density/(g·cm^{-3})	Permeability Coefficient/(cm·s^{-1})	Compression Strength/MPa	Elastic Modulus/GPa
Normal rock	2.4~2.6	4.9×10^{-3}~1.0×10^{-2}	15~20	3~5
Fault rock	1.9~2.1	5.8×10^{-4}~2.5×10^{-3}	8~12	1~1.2

4.1.2. Similarity Parameters

The similarity ratio, defined as the ratio of prototype parameter to model parameter, is essential for determining experimental parameters. Considering cost and feasibility, the similarity ratio for geometric size is set at 60, and for density, it is set at 1. The similarity ratios for other parameters can be derived based on the similarity principle, as listed in Table 10.

Table 10. The similarity relationship and ratio adopted in the model test.

Parameters	Similarity Relationship	Similarity Ratio
Geometric size C_l	—	60 (set)
Density C_γ	—	1 (set)
Displacement C_δ	$C_\delta = C_l$	60
Stress C_σ	$C_\sigma = C_l C_\gamma$	60
Strain C_ε	$C_\varepsilon = C_\delta / C_l$	1
Compression strength C_{σ_c}	$C_{\sigma_c} = C_\sigma$	60
Elastic modulus C_E	$C_E = C_\sigma / C_\varepsilon$	60
Permeability coefficient C_K	$C_K = \sqrt{C_l} / C_\gamma$	7.75

4.2. Test Device

It should be underlined that the length is defined as the extent along the tunnel axial orientation, and the width refers to the extent perpendicular to the tunnel axis in the same plane. Based on the geometric similarity ratio, the inner length of the test device is 1 m, the tunnel buried depth is 3 m, the tunnel diameter is 0.15 m, and the distance between the two tunnel centers is 0.45 m. Furthermore, to reduce boundary effects in the model tests, the distance from the device boundary to the tunnel boundary is set to be at least triple the tunnel diameter (0.45 m). As a result, the theoretical width and height of the test device should be 1.5 m and 3.6 m, respectively. Accordingly, a model test device was developed, consisting of a test container, stress loading facilities, water supply facilities, and data acquisition facilities, as illustrated in Figure 5.

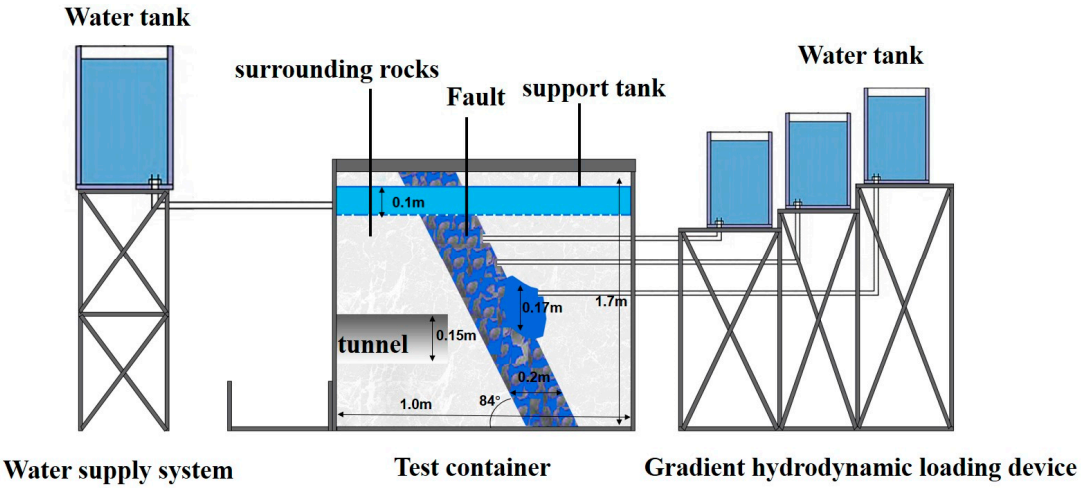

Figure 5. Model test device.

The test container with inner dimensions of 1.0 m × 1.6 m × 1.7 m (length × width × height) was used for filling the medium, and it served as the location where the disasters occurred. To restrict lateral deformations, stress-bearing columns and beams were installed around the outside of the container. Additionally, a load-bearing plate was placed at the bottom of the container to enhance its structural stability. The entire test container was constructed using 20 mm thick steel and assembled with high-strength bolts, ensuring excellent tightness, stability, and safety.

Significantly, the height of the test container was limited to 1.7 m due to constraints in test space and material cost, whereas ideally, it should have been 3.6 m to match the design value. As a result, the simulated tunnel buried depth in the model test was only 1.1 m, which was significantly less than the intended value of 3 m. To account for this discrepancy, stress loading facilities including hydraulic cylinder, controller, and pipe were used to provide an additional stress of 0.04 MPa based on engineering parameters and similarity ratios.

The water supply facilities consisted of a water storage barrel, support tank, and other ancillary equipment such as a pump and reservoir, as shown in Figure 6. To provide a constant water pressure for the test, an overflow pipe connecting with the conversation tank was installed inside the water storage barrel at a height of 1.6 m. Different constant water pressures could be achieved by adjusting the height of the support. The support tank had a size of 1.0 m × 1.6 m × 0.1 m (length × width × height) and was fixed at the top of the test container. The intake pipe, which was connected to the overflow pipe, was installed at the top of the tank, and concentrated water-permeable holes were drilled at the bottom. This setup allowed the conduit flow from the water storage barrel to be transformed into uniform flow through the water-permeable holes of the conversation tank, which then streamed into the model test. Moreover, the concentrated stress loads applied on the top of the conversation tank would be transmitted to the simulated surrounding rocks in the form of uniform loads. Finally, the pump continuously supplied water to the water storage barrel from the reservoir, ensuring that the entire test was conducted under water-rich conditions.

The data acquisition facilities consisted of osmotic pressure sensors, soil pressure sensors, displacement sensors, a static strain gauge, resistive strain brick, high-definition camera, and a collection container, as shown in Figure 7. Three monitoring sections were set up around the tunnel, and each section had five monitoring points where sensors were installed; each section had the same arrangement of sensors; ID was the displacement monitoring point. Every point around tunnel (Point 1–5) was equipped with four types of sensors, as shown in Figure 8. All sensors were pre-embedded inside the test container and connected to the static strain gauge through lead holes reserved in the test container wall. This allowed the sensors to monitor the physical and mechanical information of the corresponding

locations around the tunnel, and excavation was only performed when the monitoring data from the sensors became stable. The high-definition camera was used to record the disaster processes, and the collection container was used to collect the gushing substances.

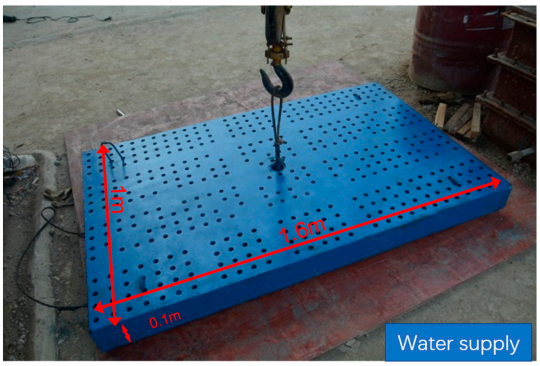

Figure 6. Support tank on the top.

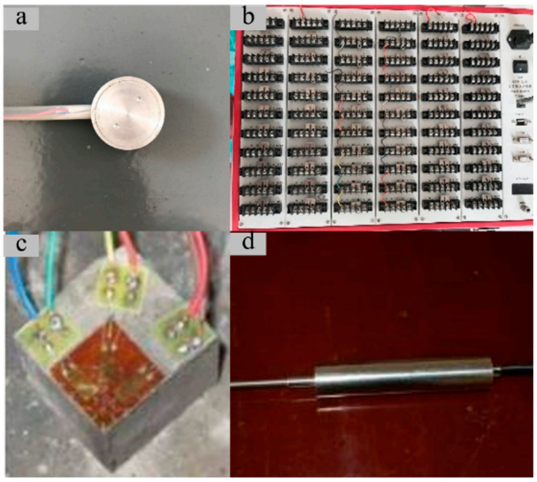

Figure 7. Data collection system. (**a**) Micro soil pressure cell. (**b**) Resistance strain analyzer. (**c**) Resistive strain brick. (**d**) Displacement sensors.

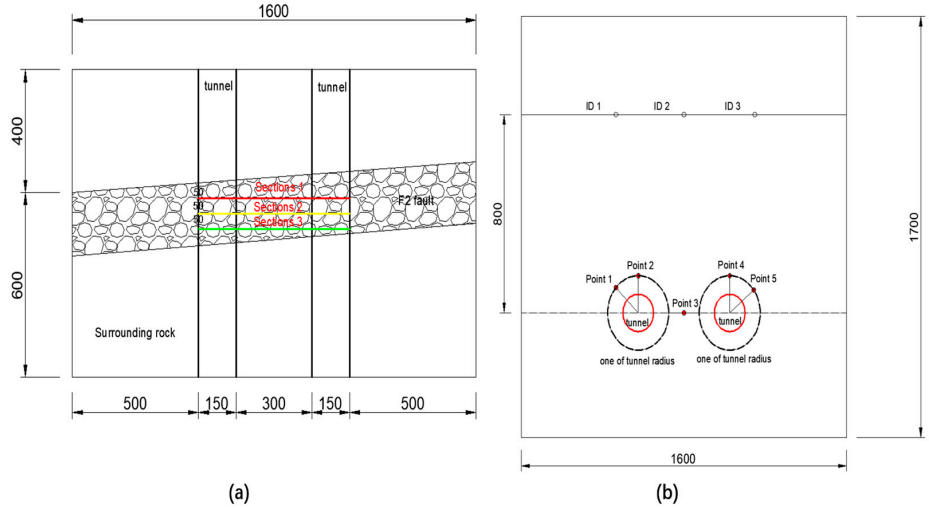

Figure 8. Layout of monitoring points. (**a**) Top view. (**b**) Layout of monitoring points in each section. ID is the displacement monitoring point. Every point around tunnel (Point 1–5) was equipped with four types of sensors, osmotic pressure sensors, soil pressure sensors, static strain gauge and resistive strain brick.

The model was excavated using the two-bench method. Initially, the excavation was divided into five steps, each 5 cm long. As the fault was approached, the excavation was divided into 30 steps, each 2.5 cm long. The tunnel was excavated sequentially from the top bench to the lower bench. The excavation process was repeated cyclically until water and mud inrush disaster occurred.

4.3. Determination of the Three Levels of Every Factor

4.3.1. Water Pressure

In this paper, the water head was used to represent the water pressure. In the actual engineering scenario, the groundwater surface with a buried depth of 50 m is 130 m higher than the tunnel vault. Accordingly, based on the stress similarity ratio, the water surface in the model test should be 2.2 m higher than the tunnel vault. Subsequently, the values of the other two levels were determined as 1.7 m and 2.7 m for test feasibility. Hence, the heights of the overflow pipe were set at 2.3 m, 2.8 m, and 3.3 m, marked as H_1, H_2, and H_3, respectively.

4.3.2. Characteristics of Similar Materials

Two types of similar materials were required for the model test. One was used to simulate the normal surrounding rocks, which needed to exhibit fluid–solid coupling characteristics and maintain feasibility under confined water conditions. The other material was meant to represent the fault-surrounding rocks and was supposed to soften and disintegrate under the effect of fluid–solid coupling. Additionally, the similar materials for the fault surrounding rocks needed to be capable of simulating different properties, as the orthogonal test required three levels of physical and mechanical properties. Therefore, a similar material marked as N was developed for the normal surrounding rocks, and three similar materials named M_1, M_2, and M_3 were developed for the fault-surrounding rocks. Detailed information about the theories and properties of these similar materials can be found in our previous works [22].

During the preparation of similar materials, the characteristic criteria of normal surrounding rocks and fault-surrounding rocks M_2 were determined first based on the parameters presented in Table 9 and the similarity ratios in Table 10. The similarity ratio for geometric size was set at 60, and for density, it was set at 1. Subsequently, the characteristic criteria of the other two similar materials, M_1 and M_3, were determined based on M_2. Finally, four similar materials were prepared by adjusting the ingredients and mass ratios to conform to their respective characteristic criteria. The ingredients and mass ratios of the four similar materials are listed in Tables 11 and 12. The main physical and mechanical properties of these similar materials were obtained through indoor tests and are summarized in Table 13.

Table 11. Ingredients and mass ratios of similar material N.

Sand	Talc	Cement	Latex	Water	Barite Powder
51.61%	22.42%	4.27%	3.79%	6.45%	11.45%

Table 12. Ingredients and mass ratios of similar materials M_1~M_3.

	Sand	Talc	Gypsum	Water	Bentonite	Paraffin Oil
M_1	68.97%	12.41%	4.83%	6.90%	5.52%	1.38%
M_2	64.52%	11.61%	9.03%	7.10%	5.16%	2.58%
M_3	61.35%	11.04%	12.27%	7.36%	4.91%	3.07%

Table 13. Main physical and mechanical properties of similar materials.

	Density/(g·cm^{-3})	Permeability Coefficient/(cm·s^{-1})	Compression Strength/MPa	Elastic Modulus/GPa
N	2.30	1.22×10^{-6}	0.60	0.08
M_1	2.03	8.84×10^{-5}	0.15	0.02
M_2	2.00	1.47×10^{-5}	0.31	0.04
M_3	1.98	5.15×10^{-6}	0.53	0.07

4.3.3. Fault Scale

In the model test, the fault scale was characterized by the fault length in the axial orientation of the tunnel. The original fault in the field, which was 18 m long (from K91 + 350 to K91 + 368), was scaled down to 0.3 m in the model test based on the geometric similarity ratio. Accordingly, three levels of fault scale were set at 0.2 m, 0.3 m, and 0.4 m for the orthogonal test, denoted as S_1, S_2, and S_3, respectively. The faults were positioned in the middle of the normal surrounding rocks and had an inclination of 84°.

In summary, the factors and their corresponding levels of the orthogonal test are summarized in Table 14.

Table 14. Factors and their corresponding levels of the orthogonal test.

Level	Water Head/m	Characteristics of Fault Rocks	Fault Scale/m
1	H_1(2.3)	M_1	S_1(0.2)
2	H_2(2.8)	M_2	S_2(0.3)
3	H_3(3.3)	M_3	S_3(0.4)

4.4. Test Scheme

The orthogonal test was designed using an orthogonal table L9 (3^4) to arrange the test conditions, as listed in Table 15. In the tests, the mass of the gushing mud was used as a qualitative indicator to denote the degree of disaster, where a larger amount of mud indicated a greater degree of disaster. The influence of factors on the disaster could be evaluated through range analysis using the disaster degrees of all test conditions.

Table 15. Arrangements of the orthogonal test.

Condition	Water Head/m	Characteristics of Fault Rocks	Fault Scale/m
T-1	H_1	M_1	S_1
T-2	H_1	M_2	S_3
T-3	H_1	M_3	S_2
T-4	H_2	M_2	S_2
T-5	H_2	M_3	S_3
T-6	H_2	M_1	S_1
T-7	H_3	M_3	S_3
T-8	H_3	M_1	S_2
T-9	H_3	M_2	S_1

In addition, the detailed procedures of the tests were as follows.

(1) To conduct the model test, the similarity materials were prepared in accordance with the test conditions, and then similar materials were filled into the model body and sensors were installed. The materials consisted of two types of rocks and were filled into different regions of the model body with controllable dip angle between the fault and normal surrounding rock. The materials were filled in layers and compacted to

achieve the design density, with each layer compacted to 1.8 cm per 10 cm. To minimize the impact of artificial stratification on the test results, each layer was polished and the fault angle was controlled using a level instrument and construction line. Once the model materials were filled to the design height, displacement sensors were placed at the monitoring points.

(2) The loading tank was placed on top of the model soil body and a top steel plate with hydraulic jacks was set on the cover and sealed with high-strength bolts. The jacks were then supported on the counter-force beam. In addition, sensors were installed at specified locations during the filling process and linked to the static strain gauge through lead holes for data collection.

(3) After filling the similar materials and embedding the sensors, the test device was assembled and sealed. Data acquisition facilities were turned on to start recording data. A compensation stress of 0.04 MPa was applied to the medium using stress loading facilities, and the support height was adjusted to the designed value to provide the required hydraulic loads for the specific test condition. To ensure a continuous water supply to the loading tank, the main water tank was connected to the loading tank through a water inlet located on the top plate.

(4) The left tunnel was excavated using the bench method once the monitoring data remained stable. The excavation parameters, which were converted based on engineering and similarity parameters, are summarized below: the height of the upper and lower benches was 6.5 cm and 8.6 cm, respectively, the bench length was 12.5 cm, and the length of each excavation step was 2.5 cm.

(5) Excavation was halted once the fault was exposed, and the disaster process was recorded while collecting the gushing substances. After the test, the gushing substances were dried to determine the mass of gushing mud. It is important to note that water may seep out during the excavation process, requiring continuous water supply to maintain the designed water head throughout the test period.

(6) The next test condition was implemented and procedures (1)~(4) were repeated.

4.5. Test Result

4.5.1. Disaster Process

All the test conditions successfully simulated mud inrush disasters, and they exhibited similar disaster processes. It is worth mentioning that all parameters of condition T-4 were determined based on actual engineering data, which means that the test condition T-4 could recreate the real disaster scenario from a model test perspective. Therefore, in this paper, condition T-4 was taken as an example to reveal the disaster process and then compared with the actual disaster process to verify the feasibility of the test.

The representative processes of test condition T-4 are depicted in Figure 7. During the test, after exposing the fault for 135 s, small bursts of currents started to flow out from the tunnel face. Gradually, the rocks surrounding the tunnel face became muddy and loose. Subsequently, collapses occurred in the tunnel face as the muddy and loose rocks struggled to withstand the water pressure and the loads from the surrounding rocks (Figure 9a). Over time, the water flowed out copiously and swiftly from the collapse site, and the range of muddy rocks expanded dramatically (Figure 9b). Eventually, the mud inrush disaster erupted, with numerous mud–water mixtures surging out instantly (Figure 9c). After the disaster subsided, a significant amount of gushing substances was left in the tunnel (Figure 9d).

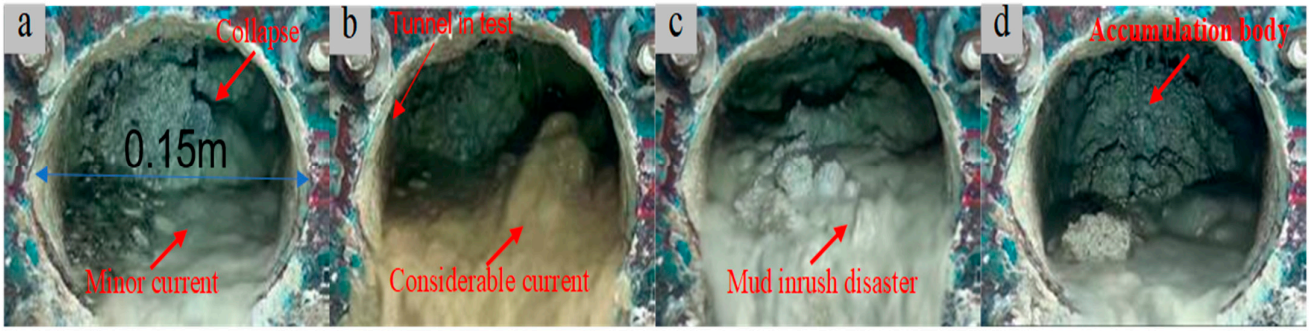

Figure 9. Representative processes of the test condition T-4. (**a**) Minor current and the collapse; (**b**) considerable current; (**c**) mud–water mixture; (**d**) accumulation body of the gushing substances.

The distinctive processes of the actual mud inrush disasters are exemplified in Figure 10. It can be concluded that the processes observed in the model tests were consistent with those observed in actual engineering scenarios. Furthermore, since the processes observed in all test conditions were essentially similar, there is sufficient evidence to support the claim that the series of model tests were able to effectively simulate mud inrush disasters under diverse circumstances.

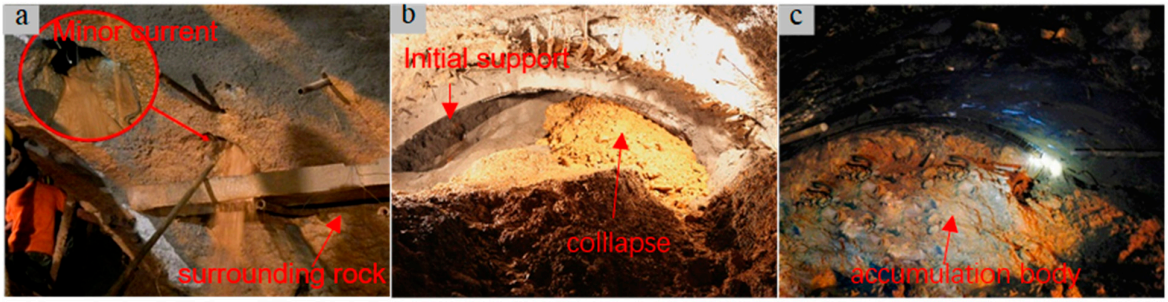

Figure 10. Distinctive actual disaster processes. (**a**) Minor current; (**b**) collapse; (**c**) accumulation body.

4.5.2. The Influence Degree of Factors

The distinctions between different test conditions were the masses of the gushing mud denoting the disaster degree; they are summarized in Table 16. Meanwhile, the parameters used for the range analysis are listed in the table as well. In Table 16, index I_j is the sum of results of test conditions containing Level 1 (Subscript 1) in column J. Similarly, indices II_j and III_j correspond to calculation values of Level 2 and 3 (Subscript 2 and 3) respectively. In addition, index k_j is the occurrence number of the identical level. Then, index D_j is the range of the Jth column, which is calculated according to the following formula:

$$D_j = max\{I_j/k_j, II_j/k_j, III_j/k_j\} - min\{I_j/k_j, II_j/k_j, III_j/k_j\}. \quad (7)$$

Index D_j denotes the influence degrees of different factors on the mud inrush disaster: the greater the value of D_j, the more significantly its corresponding factor contributes to the disaster. The results show that water pressure factor made the greatest impact on disasters followed by the characteristics of fault rocks, and the fault scale factor was of the least importance. The conclusions drawn from the model test are in concert with the above theoretical analysis.

Through the above nine sets of experiments, our newly proposed quantitative evaluation system has been sufficiently validated and demonstrated its good reference value and significance in evaluating and predicting potential mud inrush disasters in engineering. However, it should be pointed out that this new quantitative evaluation method relies heavily on the expert scoring system and may have certain subjective factors. Therefore, in the process of using this method, continuous optimization should be carried out according to the actual situation.

Table 16. Test results and the parameters of range analysis.

Condition	Water Head/m	Characteristics of Fault Rocks	Fault Scale/m	Mass of Gushing Mud/kg
T-1	H_1	M_1	S_1	129
T-2	H_1	M_2	S_3	126
T-3	H_1	M_3	S_2	105
T-4	H_2	M_2	S_2	144
T-5	H_2	M_3	S_3	120
T-6	H_2	M_1	S_1	173
T-7	H_3	M_3	S_3	160
T-8	H_3	M_1	S_2	194
T-9	H_3	M_2	S_1	167
I_j	360	496	416	
II_j	437	437	443	
III_j	521	385	459	
k_j	3	3	3	
D_j	53.67	37.00	14.33	

5. Conclusions

In order to establish a quantitative evaluation system for mud inrush disaster, we take the large-scale mud inrush disaster of Yonglian tunnel as an example and propose eight disaster-causing factors categorized into three aspects. Considering these factors, the paper introduces the Fuzzy Comprehensive Evaluation Method into the Analytic Hierarchy Process to establish a new quantitative evaluation index system for the causal factors. However, this system relies on expert judgments and may lack objectivity, A series of indoor model tests are then conducted to confirm the realism and credibility of the risk evaluation method. The results of this study demonstrate the significance of the proposed system in providing guidance and reference for the early detection and treatment of sudden mud disasters. The specific conclusions drawn from this study are as follows:

1. Through a comprehensive investigation of the mud inrush disaster in the Yonglian tunnel, we identified eight main disaster-causing factors, including terrain and groundwater pressure, which are categorized into three aspects: geological factors, hydrologic factors, and human factors. These factors effectively cover the main causes of the disaster, and a qualitative analysis of the disaster-causing mechanisms for each factor was conducted.
2. The Analytic Hierarchy Process (AHP) was employed to establish a quantitative evaluation index system for the disaster-causing factors of mud inrush disasters in water-rich fault fracture zones. The Fuzzy Comprehensive Evaluation Method was used to evaluate the secondary and primary index factors and analyze the importance and scale influence of mud inrush disaster-causing control factors. The analysis revealed that groundwater pressure, physical and mechanical properties of fault-surrounding rocks, and fault scale are the three main disaster-causing factors, with a combined total weight of 0.7081.
3. In order to verify the quantitative evaluation index system, a model test system for tunnel mud inrush disaster was established, and nine sets of tests were conducted to replicate the mud burst disaster process. The magnitude of the weights of the three groups of causal factors obtained from the model experiments was consistent with the theoretical analysis, indicating the correctness of the analytical system. This confirms the reliability and accuracy of the proposed evaluation system through practical model testing.

Author Contributions: Conceptualization, J.L. and X.Z.; methodology, X.Z. and X.L.; software, Z.L.; validation, J.L., X.Z. and X.L.; formal analysis, C.S.; investigation, J.L.; resources, Z.L.; data curation, X.L.; writing—original draft preparation, J.L.; writing—review and editing, X.Z. and X.L.; visualization, C.S.; supervision, X.Z. and J.L.; project administration, X.Z. All authors have read and agreed to the published version of the manuscript.

Funding: This research received no external funding.

Institutional Review Board Statement: Not applicable.

Informed Consent Statement: Not applicable.

Data Availability Statement: Not applicable.

Conflicts of Interest: The authors declare no conflict of interest.

References

1. Li, X.; Li, Y. Research on risk assessment system for water inrush in the karst tunnel construction based on GIS: Case study on the diversion tunnel groups of the Jinping II Hydropower Station. *Tunn. Undergr. Space Technol.* **2014**, *40*, 182–191. [CrossRef]
2. Shahriar, K.; Sharifzadeh, M.; Hamidi, J.K. Geotechnical risk assessment based approach for rock TBM selection in difficult ground conditions. *Tunn. Undergr. Space Technol.* **2008**, *23*, 318–325. [CrossRef]
3. Zhang, J.; Li, S.; Zhang, Q.; Zhang, X.; Li, P.; Wang, D.; Weng, X. Mud inrush flow mechanisms: A case study in a water-rich fault tunnel. *Bull. Eng. Geol. Environ.* **2019**, *78*, 6267–6283. [CrossRef]
4. Li, S.; Liu, B.; Xu, X.; Nie, L.; Liu, Z.; Song, J.; Sun, H.; Chen, L.; Fan, K. An overview of ahead geological prospecting in tunneling. *Tunn. Undergr. Space Technol.* **2017**, *63*, 69–94. [CrossRef]
5. Zhang, G.-H.; Jiao, Y.-Y.; Wang, H.; Cheng, Y.; Chen, L.-B. On the mechanism of inrush hazards when Denghuozhai Tunnel passing through granite contact zone. *Tunn. Undergr. Space Technol.* **2017**, *68*, 174–186. [CrossRef]
6. Zhao, Y.; Li, P.; Tian, S. Prevention and treatment technologies of railway tunnel water inrush and mud gushing in China. *J. Rock Mech. Geotech. Eng.* **2013**, *5*, 468–477. [CrossRef]
7. Ali, A.; Huang, J.; Lyamin, A.V.; Sloan, S.W.; Griffiths, D.V.; Cassidy, M.J.; Li, J.H. Simplified quantitative risk assessment of rainfall-induced landslides modelled by infinite slopes. *Eng. Geol.* **2014**, *179*, 102–116. [CrossRef]
8. Orejuela, I.P.; Toulkeridis, T. Evaluation of the susceptibility to landslides through diffuse logic and analytical hierarchy process (AHP) between Macas and Riobamba in Central Ecuador. In Proceedings of the 2020 Seventh International Conference on eDemocracy & eGovernment (ICEDEG), Buenos Aires, Argentina, 22–24 April 2020; pp. 201–207.
9. Kazakis, N.; Kougias, I.; Patsialis, T. Assessment of flood hazard areas at a regional scale using an index-based approach and Analytical Hierarchy Process: Application in Rhodope—Evros region, Greece. *Sci. Total Environ.* **2015**, *538*, 555–563. [CrossRef]
10. Alija, S.; Torrijo, F.J.; Quinta-Ferreira, M. Geological engineering problems associated with tunnel construction in karst rock masses: The case of Gavarres tunnel (Spain). *Eng. Geol.* **2013**, *157*, 103–111. [CrossRef]
11. Verma, A.; Roy, S.; Gautam, P. Estimation of groundwater seepage rate into Maneri-Uttarkashi power tunnel: An analytical approach. *Int. J. Earth Sci. Eng.* **2013**, *6*, 1429–1433.
12. Li, L.; Sun, S.; Wang, J.; Song, S.; Fang, Z.; Zhang, M. Development of compound EPB shield model test system for studying the water inrushes in karst regions. *Tunn. Undergr. Space Technol.* **2020**, *101*, 103404. [CrossRef]
13. Li, S.; Liu, C.; Zhou, Z.; Li, L.; Shi, S.; Yuan, Y. Multi-sources information fusion analysis of water inrush disaster in tunnels based on improved theory of evidence. *Tunn. Undergr. Space Technol.* **2021**, *113*, 103948. [CrossRef]
14. Idinger, G.; Aklik, P.; Wu, W.; Borja, R.I. Centrifuge model test on the face stability of shallow tunnel. *Acta Geotech.* **2011**, *6*, 105–117. [CrossRef]
15. Soranzo, E.; Tamagnini, R.; Wu, W. Face stability of shallow tunnels in partially saturated soil: Centrifuge testing and numerical analysis. *Géotechnique* **2015**, *65*, 454–467. [CrossRef]
16. Babushkina, E.A.; Belokopytova, L.V.; Grachev, A.M.; Meko, D.M.; Vaganov, E.A. Variation of the hydrological regime of Bele-Shira closed basin in Southern Siberia and its reflection in the radial growth of Larix sibirica. *Reg. Environ. Chang.* **2017**, *17*, 1725–1737. [CrossRef]
17. Meguid, M.A.; Saada, O.; Nunes, M.A.; Mattar, J. Physical modeling of tunnels in soft ground: A review. *Tunn. Undergr. Space Technol.* **2008**, *23*, 185–198. [CrossRef]
18. Yang, W.; Wang, M.; Zhou, Z.; Li, L.; Yuan, Y.; Gao, C. A true triaxial geomechanical model test apparatus for studying the precursory information of water inrush from impermeable rock mass failure. *Tunn. Undergr. Space Technol.* **2019**, *93*, 103078. [CrossRef]
19. Liu, J.; Li, Z.; Zhang, X.; Weng, X. Analysis of Water and Mud Inrush in Tunnel Fault Fracture Zone—A Case Study of Yonglian Tunnel. *Sustainability* **2021**, *13*, 9585. [CrossRef]
20. Stefanidis, S.; Stathis, D. Assessment of flood hazard based on natural and anthropogenic factors using analytic hierarchy process (AHP). *Nat. Hazards* **2013**, *68*, 569–585. [CrossRef]
21. Vaidya, O.S.; Kumar, S. Analytic hierarchy process: An overview of applications. *Eur. J. Oper. Res.* **2006**, *169*, 1–29. [CrossRef]
22. Wang, K.; Li, S.; Zhang, Q.; Zhang, X.; Li, L.; Zhang, Q.; Liu, C. Development and application of new similar materials of surrounding rock for a fluid-solid coupling model test. *Rock Soil Mech.* **2016**, *37*, 2521–2533.